Theoretical fundamentals of airframe/propulsion integration for high-speed aircraft

A. A. Gubanov

Correspondence: anatoly.gubanov@tsagi.ru
Central Aerohydrodynamic Institute named after Professor N.E. Zhukovsky (TsAGI), Zhukovsky, Moscow Region, Russian Federation

Abstract

Fundamental features of aerodynamic interference and integration of airframes and air-breathing jet engines for high-speed flight vehicles are studied within the framework of supersonic small perturbation theory. Both the influence of airframe components on air intakes performance and influence of intakes on vehicle external aerodynamics are under consideration. Analytical relations and specific examples show that significant favorable interference between airframes and air intakes can be realized by using preliminary compression of the flow in front of intakes at flight Mach numbers exceeding approximately 3.

Keywords: Aircraft aerodynamics, Supersonic flight vehicles, Aerodynamic configurations, Airframe/propulsion integration, Analytical studies, CFD, Wind-tunnel tests

1 Introduction

Effective airframe/propulsion integration is one of the principal features of advanced aerodynamic configurations used in aerodynamic design of supersonic flight vehicles with air-breathing jet engines, especially for high supersonic speeds exceeding Mach number 3. Its effects are significant for both engine thrust performance and vehicle external aerodynamics.

If some of the vehicle airframe components are used as preliminary stages of flow compression in front of intakes, their effect on intake performance appears in growth of both the intake mass flow rate and total pressure recovery coefficients. The increase in the intake mass flow rate is mainly due to the increase in the flow density. It allows using the intakes of lesser size and, correspondingly, of lesser weight for engines providing the appropriate thrust-to-drag balance of a vehicle. Preliminary compression of the flow also leads to diminution of the flow Mach number at intake entrance as compared to the Mach number in the free-stream. The latter results in higher total pressure recovery of the intake comparing with the case if an intake is located in the region of undisturbed free-stream flow. As a result, growth of total pressure recovery can considerably improve specific impulse of an engine and consequently the fuel consumption needed for flight. The example presented in Paper [1] shows that due to appropriate shaping of the forward part of the vehicle making preliminary compression more intense, both the

intake mass flow rate and pressure recovery factor could be enhanced by 30% at Mach number $M_\infty = 7$ at angle-of-attack range $0 \leq \alpha \leq 6°$ as compared to the conventional shape of the nose part having the axial symmetry.

On the other hand, if the intake is located in a disturbed flow, significant part of the drag force acting on the airframe surfaces providing flow preliminary compression before intakes could be excluded from external aerodynamic forces acting on an aircraft and considered as internal force which acts on the flow stream-tube passing through an engine. This force can be regarded as the one taking part in engine thrust generation.

In order to investigate principal relationships inherent in airframe/propulsion integration for supersonic vehicles, it is reasonable to use simplified theories, such as the linear theory of supersonic flows, i.e. the first-order approximation of supersonic small perturbation theory. The current status of CFD methods development, in particular of those based on Euler and Navier-Stokes equations, allows rather detailed and reliable aerodynamic investigations of complex configurations. However, simplified theories haven't lost their importance due to their ability of giving clear analytical relationships, which helps to understand principal features inherent in aerodynamics. Consideration of airframe/propulsion aerodynamic interference and integration within the framework of supersonic small perturbation theory gives possibility to understand a set of important trends and ways of improving aerodynamic configurations.

2 Description of the theoretical approach

The general theoretical approach used here had been described earlier in Papers [2, 3]. In order to explain the basic results, a generic configuration of high-speed vehicle shown on Fig. 1 can be considered.

Here, x and z are longitudinal and vertical co-ordinate axes, the x-axis being directed along the free-stream; S_W designates the external surface of a vehicle; $\vec{n}_W$ is a vector directed normally to the surface S_W outwards from the vehicle and having the length of unity; $\vec{\tau}_W$ is a vector of local tangential viscous stress acting on the external surface; S_1 is the surface located at the entrance section of the intake connected around its perimeter to the vehicle external surface; $\vec{n}_1$ is the vector directed normally to the surface S_1 inwards and having the length of unity; S_2 is the surface located at the exit of the internal duct nozzle connected around its perimeter to the vehicle external surface S_W;

Fig. 1 The scheme representing definition of the external aerodynamic force acting on a vehicle
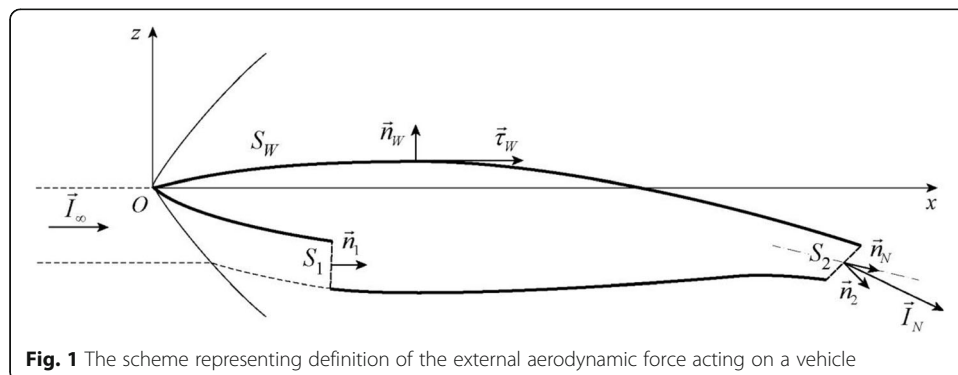
$\overrightarrow{n}_2$ is the vector directed normally to the surface S_2 outwards and having the length of unity; $\overrightarrow{I}_\infty$ is the vector of the initial momentum of the stream-tube passing through the engine; $\overrightarrow{I}_N$ is the momentum of the exit flow exhausting from the engine nozzle (or from the nozzle of the model in the case of wind-tunnel tests), and $\overrightarrow{n}_N$ is the vector of unit length directed along the nominal axis of the engine exit nozzle. To satisfy the conditions of the momentum theorem application, surfaces S_W, S_1 and S_2 should be chosen so that they form together a closed surface $S_W + S_1 + S_2$ that limits the finite volume containing the considering aircraft.

As follows from the momentum theorem, the formula for determining the resulting aerodynamic force $\overrightarrow{R}_\Sigma$ acting on an aircraft (or on its model in the case of wind-tunnel tests) can be presented in the following form:

$$\overrightarrow{R}_\Sigma = \int_{S_W} \left[-(p-p_\infty)\overrightarrow{n}_W + \overrightarrow{\tau}_W \right] dS + \overrightarrow{I}_1 - \overrightarrow{I}_N. \tag{1}$$

In this formula, p is the static pressure in the corresponding point, p_∞ is the value of static pressure in the free-stream, and $\overrightarrow{I}_1$ is a vector of intake entrance momentum defined by the formula

$$\overrightarrow{I}_1 = \int_{S_1} \left[(p-p_\infty)\overrightarrow{n}_1 + \rho(\overrightarrow{V} \cdot \overrightarrow{n}_1)\overrightarrow{V} \right] dS, \tag{2}$$

where ρ is the local density of the flow at the considering point, and $\overrightarrow{V}$ is the local flow velocity vector; the vector $\overrightarrow{I}_N$ is calculated similarly to vector $\overrightarrow{I}_1$ by integrating over the surface S_2.

According to the book-keeping principle distinguishing external and internal aerodynamic forces adopted in Russia and described, for instance, in [4], the air-breathing engine thrust (or the internal force related to the aerodynamic duct of the model) $\overrightarrow{T}$ can be represented as:

$$\overrightarrow{T} = -\left(\overrightarrow{I}_N - |\overrightarrow{I}_\infty| \overrightarrow{n}_N \right). \tag{3}$$

It is worth noting that the book-keeping principles used in different countries are slightly different. Nevertheless, the final results on airframe/propulsion integration should be similar because any particular principle leads to the same Eq. (1) for the resulting aerodynamic force $\overrightarrow{R}_\Sigma$ acting on a vehicle.

Using the definition (3) and the momentum theorem (1), the following formula can be derived for the external aerodynamic force $\overrightarrow{R}_E$ acting on a vehicle:

$$\overrightarrow{R}_E = \overrightarrow{R}_\Sigma - \overrightarrow{T} = \int_{S_W} \left[-(p-p_\infty)\overrightarrow{n}_W + \overrightarrow{\tau}_W \right] dS + \overrightarrow{I}_1 - |\overrightarrow{I}_\infty| \overrightarrow{n}_N. \tag{4}$$

In order to analyze the basic relations of airframe/propulsion integration within the framework of the supersonic small perturbation theory, viscous tension $\overrightarrow{\tau}_W$ can be excluded from consideration, as well as the influence of the vehicle nose and leading edges' bluntness. As it is accepted within the theory, the flow disturbances caused by the vehicle airframe are considered as asymptotically small (excluding the flow within

the engine duct), and the potential of the disturbed flow ϕ describing the external flow over a vehicle can be introduced, with flow velocity components V_x, V_y, and V_z along co-ordinate axes x, y, and z expressing by the formulae:

$$
\begin{aligned}
V_x &= V_\infty(1 + \phi_x); \\
V_y &= V_\infty\phi_y; \\
V_z &= V_\infty\phi_z,
\end{aligned}
\tag{5}
$$

V_∞ is the value of free-stream flow velocity. Assuming that the surface S_1 is placed approximately in the lateral plane normally to the longitudinal axis of the vehicle so that the vector $\overrightarrow{n}_1$ has longitudinal component $n_{1x} \approx 1$, and its lateral components n_{1y} and n_{1z} are asymptotically small, the resulting formulae for the external drag and lift force coefficients of a vehicle C_D and C_L within the framework of the small perturbation theory can be derived from the formula (4) as follows:

$$
C_D = C_{DW} - \frac{1}{S_{REF}} \int\limits_{S_1} \left[\left(M_\infty^2 - 1\right)\phi_x^2 + \phi_y^2 + \phi_z^2 \right] dS + \frac{F_0}{S_{REF}} f\left(\alpha_N^2 + \beta_N^2\right),
\tag{6}
$$

$$
C_L = C_{LW} + \frac{2}{S_{REF}} \int\limits_{S_1} \phi_z dS + \frac{2F_0}{S_{REF}} f\alpha_N.
\tag{7}
$$

Here, C_{DW} and C_{LW} correspond to inputs of pressure distribution over the vehicle external surface S_W into the corresponding aerodynamic coefficients, F_0 is the intake entrance area, S_{REF} is the value of the reference area used to define the considering aerodynamic coefficients, f is the intake mass flow rate coefficient, α_N and β_N are the angle-of-attack and the sideslip angle of the engine exit nozzle.

The formula for the intake mass flow rate coefficient f within the 1st order of approximation within the supersonic small perturbation theory, i.e. within the linear theory, can be expressed as follows:

$$
f = 1 - \frac{1}{F_0}\left(M_\infty^2 - 1\right) \int\limits_{S_1} \phi_x dS
\tag{8}
$$

The analytical formulae (6), (7) and (8) allow understanding the set of important relationships inherent in airframe/propulsion integration for supersonic flight vehicles.

3 Influence of vehicle airframe on intake performance

As it is seen from the Formula (8), the intake mass flow rate becomes more than unity if the longitudinal flow velocity component at the location of the air intake becomes less than the free-stream velocity. The latter corresponds to the preliminarily compressed flow capturing by the intake. Enhancement of the mass flow rate increases with growing intensity of the preliminary compression. It is a rather well-known effect. The formula helps to understand dependence of the effect from Mach number. The factor $(M_\infty^2 - 1)$ containing in the formula shows that the effect of flow preliminary compression on intake performance grows significantly with Mach number increase. For instance, in the case of an intake located in the compressed flow under a flat plate inclined at an angle-of-attack α to the free-stream, intensity of flow deceleration and compression could be characterised by the Ackeret's formula:

$$\phi_x = -\alpha / \left(M_\infty{}^2 - 1 \right)^{1/2}. \tag{9}$$

Substituting this expression into the Formula (8) and assuming that the flow at the intake location is uniform, the formula for the intake mass flow rate becomes as follows:

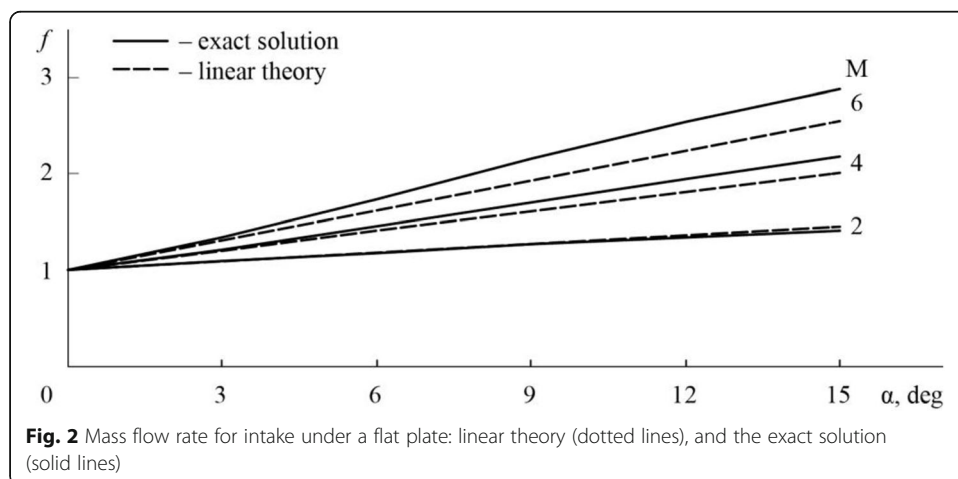$$f = 1 + \alpha \left(M_\infty{}^2 - 1 \right)^{1/2}. \tag{10}$$

It means that if angle-of-attack α is fixed, the mass flow rate coefficient grows significantly with increasing Mach number.

The Formula (8) is asymptotic. It means that theoretically it is valid just for the cases if perturbations of flow parameters are small. Nevertheless, it is worth to be mentioned that the practical range of its possible use is rather wide, because really relationships of the intake mass flow rate from angle-of-attack at fixed supersonic Mach numbers are close to linear ones. Relationships $f(\alpha)$ corresponding to the considering case obtained both from the Formula (10) and from exact solution for compressible supersonic flows at fixed Mach numbers are depicted on Fig. 2.

It is seen from the figure that linear theory gives rather appropriate approximation for the intake mass flow rate at $M_\infty \leq 4$ in the whole considering range of angle-of-attack $\alpha \leq 15°$. If $M_\infty = 6$, significant discrepancies exceeding 10% occur at $\alpha \geq 6°$.

4 Airframe/propulsion integration in terms of external aerodynamics

In practical cases, if the intake is designed properly, the shock-waves causing by its own compression ramps at the most important parts of flight trajectory of a vehicle should not lead to considerable spillage of the compressed flow, and the influence of these ramps on vehicle external aerodynamics should not be significant. In such cases, vehicle external aerodynamics can be considered without taking into account components of an intake which influence just on internal flow. Exclusion of the intake compression ramps from consideration in external aerodynamics analysis of a vehicle allows us to evaluate the pure effects of airframe/propulsion integration related to arrangement of airframe components and intakes, not mixed with the influence related to particular intake design.

Fig. 2 Mass flow rate for intake under a flat plate: linear theory (dotted lines), and the exact solution (solid lines)
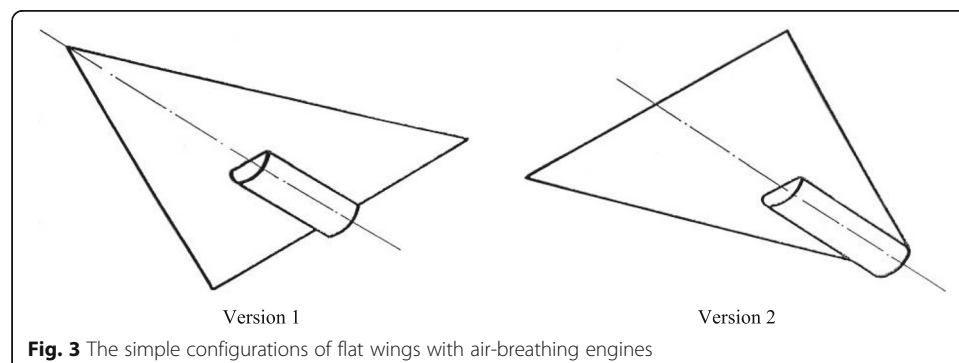
Both interesting and practically important relationships follow from qualitative consideration of Formulae (6) and (7) for external drag and lift force coefficients.

First of all, it should be noted that, following from the Formula (6), if an intake is located in a disturbed flow, it always leads to diminution of vehicle external drag. Really, the additional term in the Formula (6) related to influence of airframe/propulsion interference includes the terms of flow velocity disturbances squared with the 'minus' sign. It means that the external drag force of the whole vehicle is always less than the corresponding component of force acting on its external surface, no matter what kind of flow disturbance at the intake entrance location is: deceleration or acceleration. In order to improve both external aerodynamics and intake performance, it is reasonable to choose preliminary deceleration (and compression) of the flow.

Another important effect follows from the factor $(M_\infty^2 - 1)$ in the term containing ϕ_x^2. Due to this factor, the influence of this term on the external drag force grows sharply with increasing Mach number. Considering again the above mentioned case of an intake located under a flat plate, ϕ_x being expressed by the Formula (9), one can see that this term in the considering case does not depend from Mach number. Taking into account that absolute values of aerodynamic coefficients usually diminish with increasing Mach number in the supersonic range, in linear theory proportionally to $(M_\infty^2 - 1)^{-1/2}$, relative growth of the considering effect of airframe/propulsion interference on vehicle external aerodynamics becomes evident.

Interesting example of airframe/propulsion integration influence on rational shaping of airframe components had been considered in the Paper [2]. The example includes consideration of the two different simplified schemes of vehicles with air-breathing engines shown on Fig. 3. Each of the considering vehicles consists of a triangular wing with 'sonic' side edges, and an air-breathing jet engine with a cylindrical external surface. The difference is that the wing of the 1st vehicle (Version 1) meets the free-stream flow by its apex, and the wing of the 2nd one (Version 2), by its bottom. Intakes are supposed to be rather small so that the flow parameters at the intake entrance in the 1st case could be considered as uniform. Both vehicles are considering as flying at the same angle-of-attack α, and the engine exit nozzles in both cases are supposed to be parallel to the wing plane and to the plane of symmetry, i.e. $\alpha_N = \alpha$ and $\beta_N = 0$.

According to the reverse flow theorem, aerodynamic forces acting on isolated wings of the two versions are similar: $C_{DW1} = C_{DW2} = C_{DW}$; $C_{LW1} = C_{LW2} = C_{LW}$ in terms of

Version 1   Version 2

Fig. 3 The simple configurations of flat wings with air-breathing engines

Formulae (6) and (7). Application of the linear theory to consideration of flow-fields around the configurations gives the expressions for longitudinal velocity disturbances ϕ_x for both cases as follows:

$$\phi_{x1} = -2\alpha/\pi\left(M_\infty{}^2-1\right)^{1/2};$$
$$\phi_{x2} = -\alpha/\left(M_\infty{}^2-1\right)^{1/2}. \tag{11}$$

In the 2nd case the flow preliminary compression is stronger, and it provides stronger impact on the external drag of the vehicle. The vertical component of the disturbed flow velocity ϕ_z, according to the boundary conditions on the wings surfaces, for both cases equals to angle-of-attack with the 'minus' sign:

$$\phi_{z1} = \phi_{z2} = -\alpha. \tag{12}$$

Using the Formula (6) and the values of flow velocity disturbances (11) and (12), the external drag force coefficients for the considering configurations can be expressed as:

$$C_{D1} = C_{DW} - (2/\pi)^2\alpha^2 F_0/S_{REF};$$
$$C_{D2} = C_{DW} - \alpha^2 F_0/S_{REF}. \tag{13}$$

The corresponding expression for the lift force coefficients is the following:

$$C_{L1} = C_{L2} = C_{LW}. \tag{14}$$

As it is seen from the Formulae (13) and (14), the external drag force of the 2nd vehicle is less as compared to that of the 1st one, the lift force of both vehicles being equal. The absolute value of the negative additional term related to airframe/propulsion integration in the 2nd expression of (13) for C_{D2} is $(\pi/2)^2 \approx 2.5$ times larger than that in the 1st one for C_{D1}. It means that the airframe/propulsion interference in the 2nd case is significantly more favourable, and the lift-to-drag ratio of the 2nd version of a vehicle is higher as compared to that of the 1st one.

The latter conclusion can be generalized so that the airframe/propulsion integration for high-speed aerial vehicles leads to significant change of conventional ideas on choice of the rational aerodynamic shapes: according to the reverse flow theorem, the considering isolated wings have the same aerodynamic force coefficients, while their aerodynamic characteristics in combinations with air-breathing engines become different.

5 Examples of the integrated aerodynamic schemes

As it is seen from the considered above relationships, the advanced aerodynamic configurations of high-speed vehicles with air-breathing jet engines can be based on the concept of providing the intense preliminary compression of the flow before air intakes. The well-known configurations of such vehicles include American flight test vehicles X-43A and X-51A. These vehicles use their nose parts that have flat bottom surfaces to provide flow preliminary compression.

The other possible integrated aerodynamic schemes of vehicles studied in the Central Aerodynamic Institute named after Professor N.E. Zhukovsky (TsAGI) include those based on using the classical waverider and Busemann biplane concepts. These two configurations described also in [3, 5] were developed and investigated both theoretically

and experimentally by the author of this paper in cooperation with TsAGI specialists M.F. Pritulo, V.M. Ruch'ev, V.V. Kovalenko, V.V. Khlevnoy, and D.Yu. Gusev.

The first of the configurations is based on the concept of waverider [6, 7] which is well-known as the very promising one for obtaining high aerodynamic efficiency. The classical waverider has the form of a caret wing with leading edges lying on the surface of oblique shock wave creating uniform compressed flow. The nose part of the configuration considering here consists of the two caret lifting elements connected by their upper surfaces and providing intense preliminary compression of the flow before the two intakes. The scheme of possible vehicle configuration and the photo of its model which has been tested in the TsAGI wind tunnel T-116 are presented on Fig. 4 (the part of the configuration simulating by the model for aerodynamic tests is designated on the figure by the letter L).

The configuration was designed for cruise Mach number 5. CFD calculations of local flow parameters around the nose part of the considering waverider configuration were performed by numerical solution of the stationary 3D-Euler equations using the program described in [8]. The results obtained for the regime $M_\infty = 5$ and angle-of-attack of the model $\alpha = 6°$ are shown in Fig. 5 which represents the cross-sectional distributions of the local Mach number M_l and the mass flow function

$$f_l = \rho_l u_l / \rho_\infty V_\infty, \tag{15}$$

ρ_l and u_l are local density and longitudinal flow velocity, ρ_∞ and V_∞ are density and flow velocity values in the free stream.

It is seen from the Figure that preliminary flow compression provided by the waverider is intense, and the uniformity of the flow-fields in the main regions of the compressed flow (except the vicinities of the leading edges) is high. The local Mach number in the main parts of the compressed flow at the anticipated areas of intake entrances equals approximately to 4, and the mass flow function which characterizes the expecting value of the intake mass flow rate coefficient approaches to 2. It means that characteristics of intakes located in the compressed flow near considering waverider such as the mass flow rate coefficient and the total pressure recovery factor could be significantly higher as compared to those of intakes located in undisturbed flow.
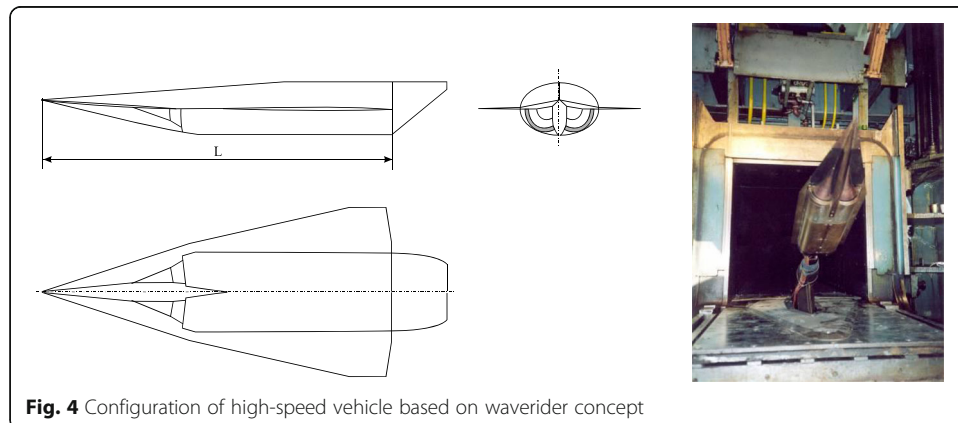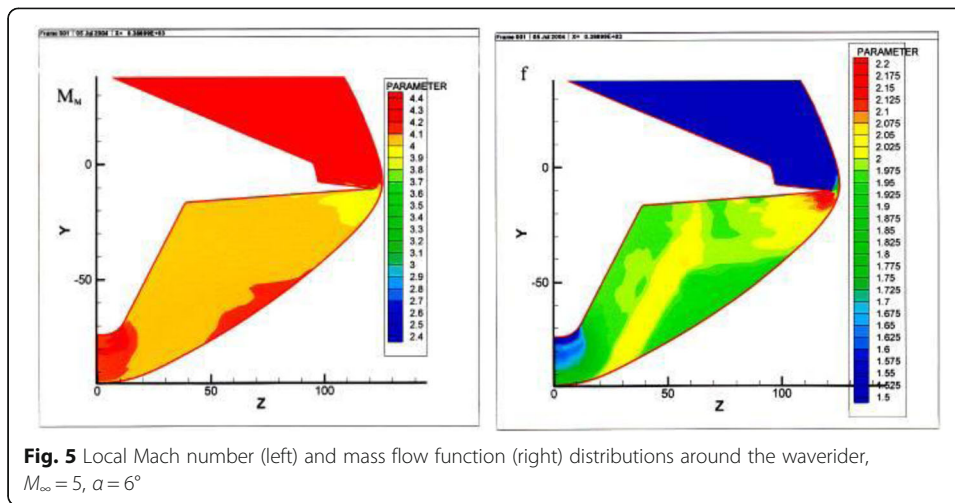

Fig. 4 Configuration of high-speed vehicle based on waverider concept

Fig. 5 Local Mach number (left) and mass flow function (right) distributions around the waverider, $M_\infty = 5$, $\alpha = 6°$

The tests of the model were conducted in the wind tunnel T-116 of TsAGI at Mach number $M_\infty = 5$ and the Reynolds number $Re_L = 6\cdot10^6$ calculated for the model length $L = 900$ mm. The range of the model angle-of-attack change was $\alpha = -4°...20°$. When determining the aerodynamic coefficients, the middle section of the model body $S_m = 19,240$ mm^2 was used as the characteristic area; the intake mass flow rate coefficient was calculated using the entrance area of a single intake $F_0 = 3$,831.6 mm^2 as a characteristic value.

The model demonstrated high lift-to-drag ratio: for its variant with the outer wings area related to the area of the body mid-section $S_w/S_m = 2.24$ and with the central bodies of intakes corresponding to the design Mach number $M_d = 3.5$, the maximum value of lift-to-drag ratio $(L/D)_{max}$ obtained in wind-tunnel tests reached approximately 5.3.

Comparison of the CFD results with the experimental data on external drag force coefficient C_D, the lift force coefficient C_L, lift-to-drag ratio L/D, and intakes mass flow rate f is given in Fig. 6. CFD calculations were provided as described in the Ref. [8]: the local flow-fields around the considering configuration and the pressure distribution over its external surface were obtained by numerical integration of 3D-Euler equations, and the skin friction drag force was evaluated using the engineering technique based on simplified formulae for the friction drag on the flat plate. The friction drag was calculated taking into account the values of local flow parameters obtained by solving the 3D-Euler equations, and laminar-to-turbulent transition of the boundary layer was supposed to take place at the line corresponding to local Reynolds number $Re_l = 10^6$.
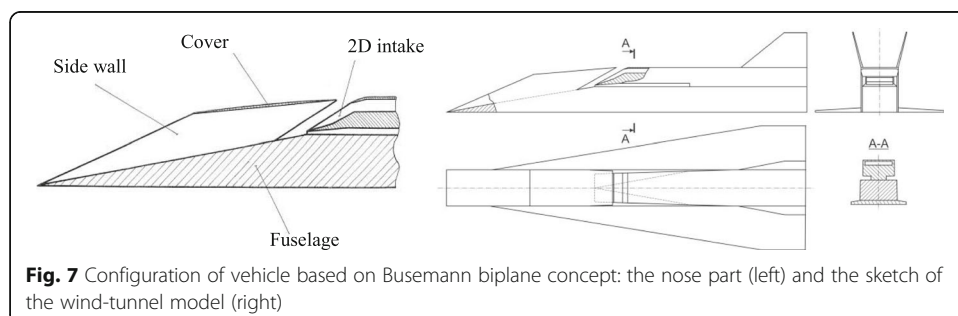
Based on the presented data, it is possible to make a conclusion on quite good agreement of CFD results obtained by using the above-mentioned methodology for the considering configuration with the results of wind-tunnel tests.

The second advanced vehicle configuration was based on the Busemann biplane concept. This concept is known from 1936 [9]. The advantage of the Busemann biplane is that it has a volume and theoretically does not produce any wave drag. But, if compared with conventional aerodynamic shapes, the biplane configurations

Fig. 6 Comparison of CFD results with the experimental data
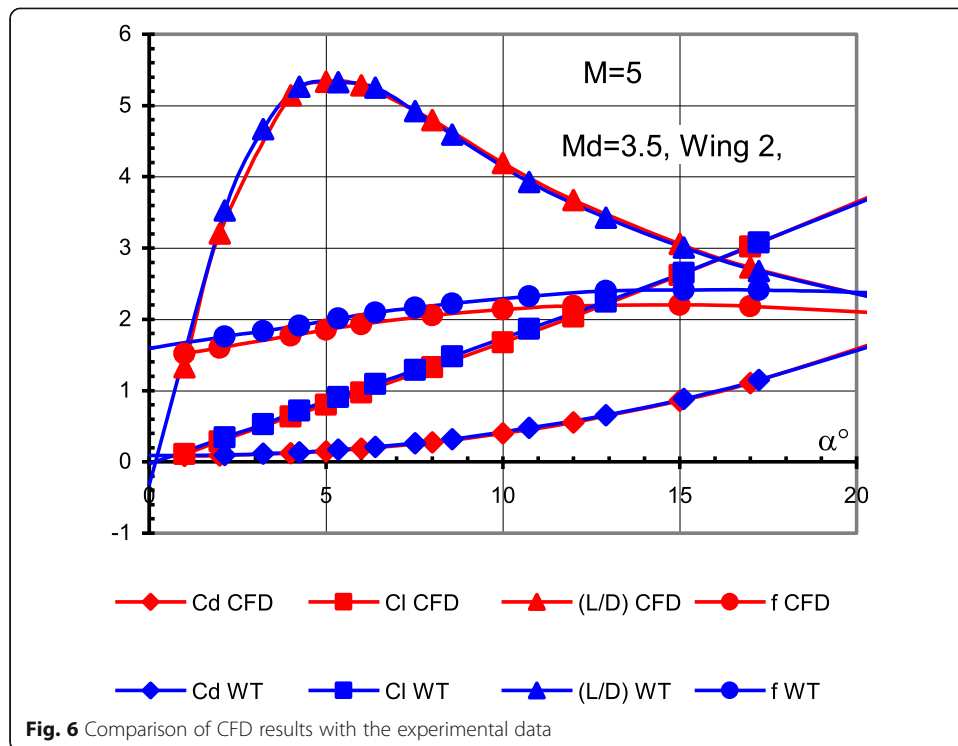
have approximately doubled area of their surfaces, and it leads to doubled skin friction drag. It is the reason why the classical Busemann biplane configuration had not found its practical application until now. If used in the design of vehicle with air-breathing jet engine, the Busemann biplane acquires additional advantage of forming the area of efficiently compressed flow passing through two oblique shock waves. This area could be extremely comfortable for positioning of the air intakes. The latter circumstance allows us to reconsider the question on possible use of the concept.

Configuration of possible vehicle developed and tested in TsAGI is presented on Fig. 7. It has been designed for cruise Mach number 4. Preliminary compression of the flow before conventional 2D intake is provided by the two surfaces: the upper surface of the nose part of vehicle fuselage, and the bottom surface of the flat cover which is installed on two side walls preventing spatial spillage of the compressed flow. The slots in front of the leading edges of the intake shown at the picture and boundary layer diverter system between the fuselage and the 2D intake

Fig. 7 Configuration of vehicle based on Busemann biplane concept: the nose part (left) and the sketch of the wind-tunnel model (right)

are necessary to ensure the starting of supersonic flow inside the biplane configuration.

At the design flow conditions ($M_\infty = 4$, $\alpha = 5°$), the pre-compression device deflects the free-stream flow up and then down by the same angles of 5°. As a result of such pre-compression, the local flow Mach number at the intake location is reduced from 4 to 3.3, and the estimated value of the mass flow rate coefficient calculated without taking into account the effects of viscosity is $f_c = 1.83$.

The model tests in TsAGI wind tunnels SVS-2 and T-116 have shown that the supersonic flow in the device under consideration started at Mach numbers $M_\infty = 2.5$ and higher, and the maximum value of the aerodynamic efficiency $(L/D)_{max}$ at the design Mach number $M_\infty = 4$ and the Reynolds number $Re_L = 20 \cdot 10^6$ equals approximately to 4.7, see Fig. 8. It is a rather high value, taking into account necessity of using the boundary layer diverter system between the body and the intake.

The value of maximum lift-to-drag ratio obtained for this model $(L/D)_{max}$ is lower as compared to that obtained for the vehicle design based on waverider. However, due to more intense flow pre-compression it can provide higher performance of the air intake. For this model, the experimental studies of the intake throttling characteristics were performed in TsAGI SVS-2 wind tunnel at Mach numbers $M_\infty = 4$, 4.5 and 5. The results of these studies are presented in Fig. 9 in the form of dependences of maximum values of the intake mass flow rate coefficient f and the total pressure recovery factor $v = p_t/p_{t\infty}$ vs. angle-of-attack of the model α.

The presented results show that the considering configuration allows getting very high performance of the air intake, which is extremely difficult to reach by use of traditional technical solutions.
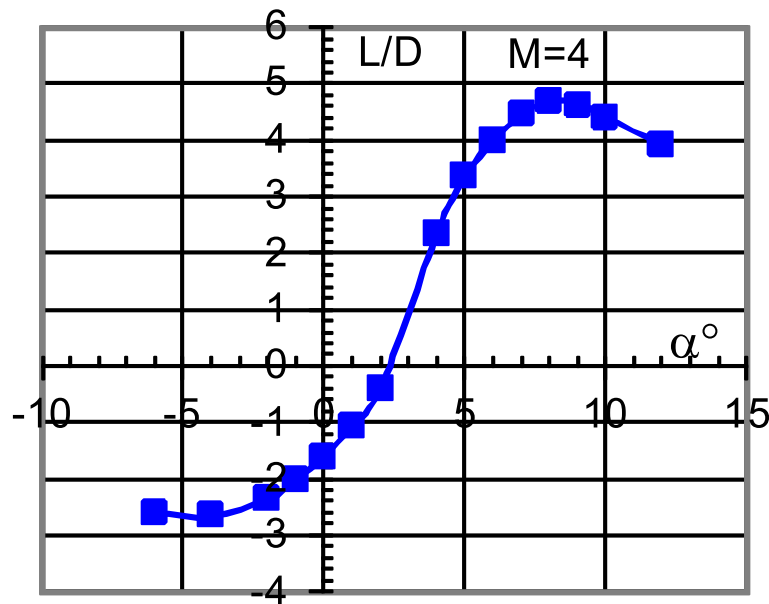

Fig. 8 The results of wind-tunnel tests of the vehicle based on the Busemann biplane concept: aerodynamic efficiency, *L/D* vs. angle-of-attack *a*

Fig. 9 The results of experimental study of the air intake throttling characteristics for the design based on the Busemann biplane concept: maximum values of the intake mass flow rate coefficient f and of the total pressure recovery factor ν vs. angle-of-attack of the model α
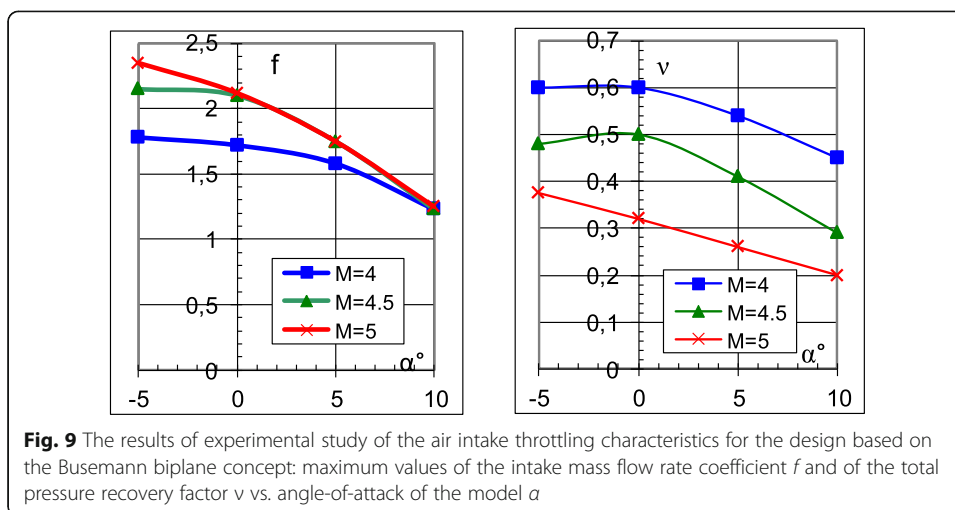
Interest in the possibility of using unconventional aerodynamic shapes, such as waveriders and biplanes, in the design of high-speed aircraft is currently maintained, as evidenced, for example, by recent developments [10–13].

6 Conclusion

1. The study has confirmed ability of using theoretical approaches based on small perturbation theory to assist researchers in the study of fundamental relationships inherent in airframe/propulsion aerodynamic interference and integration.
2. As follows from the analytical relations derived, aerodynamic interference of vehicle airframe with air intakes becomes stronger with increasing Mach number.
3. Analytical study supports the expedience of using the intense preliminary compression of the flow before air intakes by airframe components. As a result of its use, both intake performance and vehicle external aerodynamics could be improved significantly.
4. Analysis of the simple combinations of wings and air-breathing jet engines shows that airframe/propulsion integration leads to significant change of the conventional ideas on aerodynamic optimization.
5. Consideration of aerodynamic configurations based on classical concepts of waverider and Busemann biplane shows that their use allows reaching high values of lift-to-drag ratio, intake mass flow rate, and total pressure recovery.

Author's information
Anatoly A. Gubanov, Candidate of Technical Sciences, TsAGI, author of over 80 scientific publications. Research interests include airframe/propulsion integration for high-speed aircraft.

Competing interests
There are no financial or non-financial competing interests in the publication of the article.

Publisher's Note
Springer Nature remains neutral with regard to jurisdictional claims in published maps and institutional affiliations.

References
1. Bissinger NC, Blagoveshchensky NA, Gubanov AA et al (1998) Improvement of forebody/inlet integration for hypersonic vehicle. Aerospace Science and Tecynology (8):505–514
2. Gubanov AA, Pritulo MF, Ruch'yev VM (1994) Theoretical investigation of airframe/inlet interference and integration for hypersonic vehicles. Zeitschrift für Flugwissenschaften und Weltraumforschung 18:379–382
3. Gubanov AA (2013) Fundamental relations on airframe/propulsion aerodynamic integration for supersonic aircraft. *5th European Conference for Aeronautics and Space Sciences (EUCASS).* Munich, Germany, 1–5 July 2013
4. Blishch VG (1987) External and internal aerodynamic forces and moments of air-breathing jet powered vehicles and their models at incidence and sideslip. Trudy TsAGI, Issue 2328 *(in Russian)*
5. Gubanov AA, Gusev DYu (2014) Potential use of waverider and Busemann biplane in aerodynamic design of high-speed vehicles with air-breathing engines. *29th Congress of the International Council of the Aeronautical Sciences.* St.-Petersburg, Russia, 7–12 Sept 2014
6. Maikapar GI (1959) Wave drag of non-axisymmetric body in supersonic flow. J Appl Math Mech 23(2) *(in Russian)*
7. Nonweiler TRF (1959) Aerodynamic problems of manned space vehicles. J Royal Aeron Society 63(585)
8. Kovalenko VV, Khlevnoy VV (1992) Complex of computer codes for calculating the supersonic flow over vehicles. *Proc. Second Sino-Russian Symposium on Aerodynamics,* Beijing, 1992
9. Busemann A (1936) Aerodynamicher Auftrieb bei Überchallgeschwindigkeit. *Atti del 5 Convegno Volta "Le alte velocità in aviazione".* Roma, Reale Accademia d'Italia, 1936
10. Steelant J, Langener T (2014) The LAPCAT-MR2 hypersonic cruiser concept. *29th Congress of the International Council of the Aeronautical Sciences,* St.-Petersburg, Russia, 7–12 Sept 2014
11. X Xiang, Yuan L, Zhansen Q (2017) Investigation of a wide range adaptable hypersonic dual-Waverider integrative design method based on two different types of 3D inward-turning inlets. *21st AIAA International Space Planes, Hypersonic Systems and Technologies Conference,* Xiamen, China, 6–9 March 2017
12. Yi-qing Li, Xiao-gang Z, Teng J, Yan-Cheng Y (2017) Dual Waverider concept for inlet-airframe integration with Controllable Wall pressure distribution. *21st AIAA International Space Planes, Hypersonic Systems and Technologies Conference,* Xiamen, China, 6–9 March 2017
13. Kai C, Yao X, YingZhou X, GuangLi L (2018) Hypersonic I-shaped aerodynamic configurations. Science China Physics, Mechanics & Astronomy 61(2):014722